RSC Advances

ROYAL SOCIETY OF CHEMISTRY

www.rsc.org/advances

Facile fabrication and enhanced gas sensing properties of hierarchical MoO_3 nanostructures

Huihui Yan, Peng Song *, Su Zhang, Zhongxi Yang, Qi Wang

School of Material Science and Engineering, Shandong Provincial Key Laboratory of Preparation and Measurement of Building Materials, University of Jinan, Jinan 250022, China

Graphical abstract

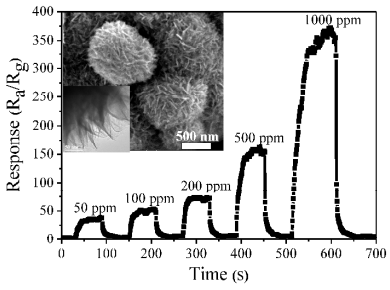

Hierarchical MoO_3 nanostructures, synthesized through oxidization conversion of hydrothermally synthesized MoS_2 precursors, show superior gas sensing performance toward ethanol.

Journal Name

ARTICLE

Facile fabrication and enhanced gas sensing properties of hierarchical MoO_3 nanostructures

Received 00th January 20xx,
Accepted 00th January 20xx

DOI: 10.1039/x0xx00000x

www.rsc.org/

Huihui Yan, Peng Song *, Su Zhang, Zhongxi Yang, Qi Wang

Hierarchical nanostructures are very promising gas-sensing materials due to their well-aligned structures with less agglomerated configurations. In this paper, hierarchical MoO_3 nanostructures were successfully synthesized through the oxidization conversion of hydrothermally synthesized MoS_2 precursors. The morphology and microstructure were characterized by X-ray diffraction (XRD), field emission scanning electron microscopy (FESEM), thermogravimetric and differential scanning calorimeter analysis (TG-DSC), transmission electron microscopy (TEM), X-ray photoelectron spectra (XPS), and N_2 adsorption-desorption analyses. The results clearly reveal that MoS_2 precursors can completely transfer into MoO_3 *via* the annealing process at 400 ^{o}C. And the as-prepared hierarchical MoO_3 nanostructures are about 500 nm in diameter, which are constructed by relatively densely packed nanosheets with the thickness of around 5-10 nm. Based on the experimental results, a possible mechanism for the formation of hierarchical MoO_3 nanostructures was speculated. Furthermore, owing to the well-defined and uniform hierarchical structure, the sensor based on hierarchical MoO_3 nanostructures shows superior gas sensing performance towards ethanol and it maybe has potential application in the detection of ethanol vapors.

Introduction

Metal oxide semiconductor gas sensors have attracted a wide range of attentions because of their low cost, flexibility associated to their production, compatible with electronic systems, the simplicity of their applications in toxic and volatile gases detection.[1-3] Molybdenum trioxide (MoO_3), as an important n-type semiconductor with a band gap of approximately 2.39-2.9 eV, has been widely used in various applications, such as gas sensors, energy storage and catalysis.[4, 5] To enhance the functional properties of MoO_3 nanostructures, it is essential to control its size and morphology. Especially for application as gas sensors, high surface to volume ratios and nanoscale dimension are the key factors to determine the gas response.[6] Based on above traits, considerable efforts have been devoted to synthesis of MoO_3 nanostructure material with different morphologies, such as lamellar, hollow microspheres, thin films, nanoparticles, nanorods and nanosheets by using thermal evaporation, spray pyrolysis, reactive sputtering, infrared irradiation heating, hydrothermal and solvothermal method.[7-12] Obviously, the synthesis of MoO_3 nanostructures with well-controlled morphology is important for uncovering their morphology-dependent properties and for achieving their practical applications. For instance, Bai et al. have prepared α-MoO_3 nanorods with high sensitivity performances to CO.[13] Kim et al. synthesized MoO_3 nanoparticles by solvothermal method, and the nanoparticle MoO_3 gas sensor exhibited high gas response toward H_2S with a short response time.[14]

Being a special kind of nanostructure, three dimensional (3D) hierarchical nanostructures have become strategic for various applications mainly due to their large specific surface area and desirable surface permeability.[15] Actually, these favorable properties are also significant for gas sensing, which can allow fast diffusion for target gases to interact with the entire sensing layer.[16-19] For instance, Wang et al. have prepared α-Fe_2O_3 hierarchical nanostructures with improved sensor performances in comparison with the compactα-Fe_2O_3 structures.[20] Lin et al. synthesized hierarchically assembled 3D porous ZnO through the calcination of zinc hydroxide carbonate precursor, which showed improved ethanol response compared to 2D porous ZnO nanoplates.[21] S. Agarwala et al have tried to develop hybrid a-Fe_2O_3 flower-like morphology which exhibits both superior electron transport and high surface area.[22] They also have been achieved high yield of 3D tin oxide sea-urchin nanostructures via an economical hydrothermal process without the use of any physical template.[23] However, there are few reports about hierarchical MoO_3 nanostructures. Hence, it is strongly desirable for the fabrication of the porous MoO_3 hierarchical nanostructures by exploring more simple and effective techniques.

Herein, we develop a facile two-step strategy to design and fabricate MoO_3 hierarchical architecture by the oxidization conversion of hydrothermally synthesized MoS_2 precursors. To our best knowledge, such MoO_3 nanostructure has rarely been reported. The obtained hierarchical MoO_3 nanostructures consisted of a number of two dimensional (2D) MoO_3 nanosheets. The present method is facile, fast, economical, and environmentally friendly. With the structural advantage, the as-synthesized hierarchical MoO_3

School of Material Science and Engineering, Shandong Provincial Key Laboratory of Preparation and Measurement of Building Materials, University of Jinan, Jinan 250022, China. E-mail: mse_songp@ujn.edu.cn

nanostructures are expected to manifest enhanced gas sensing properties.

Experimental

Synthetic procedures

All the chemical reagents were analytical graded and used without further purification. The MoS_2 precursors were synthesized through a simple hydrothermal method. In a typical reaction, 2 mmol of sodium molybdate ($Na_2MoO_4 \cdot 2H_2O$) and 9 mmol of thiocarbamide (CH_4N_2S) were mixed and dissolved in 70 ml deionized water. After stirring the solution for 30 min, 2.2 mmol of citric acid ($C_6H_8O_7 \cdot H_2O$) was added into the above solution. After magnetically stirring for 10 min, the homogeneous solution was transferred into a 100 ml Teflon-lined stainless steel autoclave, sealed tightly, and maintained at 200 ^oC for 21 h. After the hydrothermal procedure, the autoclave cooled down to room temperature spontaneously. The black precipitates were collected by centrifugation, washed several times with deionized water and absolute ethanol, respectively, and dried at 60 ^oC for 12 h in air. Finally, hierarchical MoO_3 nanostructures were obtained by calcining MoS_2 precursors at 400 ^oC for 3 h in air. The heating rate was controlled at 1 ^oC/min.

Characterization

The crystal structure and phase composition of as-prepared samples were identified by powder X-ray diffraction (XRD, Bruker D8 Advance) using Cu*Ka*1 radiation (λ = 0.15406 nm) at 30 kV and 40 mA at a scanning rate of 2^o at 2θ min^{-1}. The morphology and nanostructure of the products were characterized using FEI Sirion 200 field emission gun scanning electron microscope (FESEM, Hitachi S4800), and transmission electron microscopy (TEM, Hitachi H-800). More details about the structure were investigated by the selected area electron diffraction (SEAD) pattern and high resolution transmission electron microscopy (HRTEM, JEOL 2010). Thermogravimetry–differential scanning calorimetry (TG-DSC, Mettler-1600HT, Sweden) was used to analyze the variation of heat and weight while the precursors were being annealed. The specific surface area was estimated using the Brunauer–Emmett–Teller (BET) method based on the N_2 adsorption-desorption tests. Pore-size distribution was calculated from the adsorption branch of the nitrogen isotherm, using the Barrett–Joyner–Halenda method applied to the desorption part of the adsorption-desorption isotherm. X-ray photoelectron spectra (XPS) were measured using a PHI 5300 X-ray photoelectron spectrometer with Al K*a* radiation.

Gas sensor fabrication and response tests

The fabrication progress of the gas sensor was as follows: the as-obtained final product was ground and mixed with deionized water in order to form paste in agate mortar, which was evenly smeared onto the outer surface of a ceramic tube by hair brush to form a thick film to cover a pair of Au electrode, which had been printed on the tube previously. Four Pt lead wires attaching to the Au electrodes were used for measurement and a Ni-Cr alloy coil through the tube as a heater to operating the temperature. After dried in the air and aged at aging set at 2 days, it has been an indirectly-heated gas sensor, and then the gas sensor was put into the test chamber in a measuring system of WS-30A (Winsen Electronics Co. Ltd., Zhengzhou, China) by a static process. Then, the sensors were put into a glass chamber at the beginning. When the resistances of all the sensors were stable, the calculated amount of the target gas or liquid was injected into glass chamber by a micro-injector and mixed with air. After the sensor resistances reached a new constant value, the test chamber was opened to recover the sensors in air. All the measurements were performed in a laboratory fume hood with a large draught capacity. The sensor resistance and response values were acquired by the analysis system automatically. The whole experiment process was performed in a super-clean room with the constant humidity and temperature. In the test process, a working voltage of 5 V ($V_{working}$) was applied. By monitoring the voltage across the reference resistor (V_{output}), the response of the sensor in air or in a test gas could be measured. The sensor response was defined as:

$$Response = R_{air}/R_{gas} \quad (1)$$

where R_{air} is the resistance of the sensor in air and R_{gas} is the resistance of sensor in the presence of the test gas. The response and recovery time was defined as the time taken by the sensors to achieve 90% of the total resistance change in the case of adsorption and desorption, respectively.

Results and discussion

Crystal structure and morphology

The crystal structure of the prepared MoS_2 and MoO_3 were characterized by X-ray diffractometer. As shown in Fig. 1, the diffraction peaks of the MoS_2 precursors are in good agreement with hexagonal MoS_2 (JCPDS card no. 37-1492) without any detectable impurities. The hierarchical MoO_3 nanostructures were synthesized by annealing hydrothermally obtained MoS_2 precursors. The XRD patterns of as-synthesized hierarchical MoO_3 nanostructures could be well indexed with the standard card (JCPDS card no. 35-0609). There are no impurities observed in the XRD patterns, which indicates that MoS_2 precursors can completely transfer into MoO_3 *via* the annealing process.

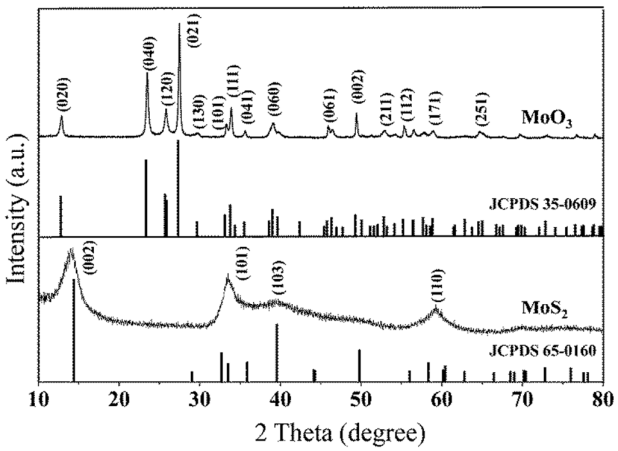

Fig. 1 XRD patterns of as-prepared MoS_2 precursors and hierarchical MoO_3 nanostructures.

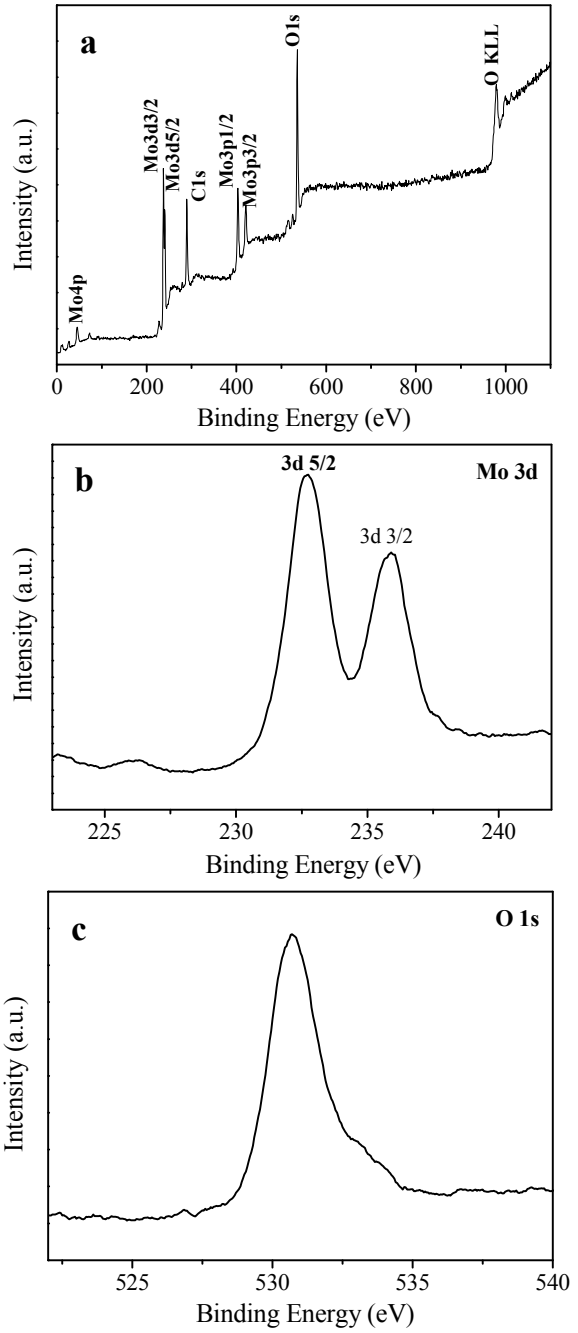

Fig. 2 XPS results of as-prepared MoO_3 samples: (a) survey spectrum, (b) Mo 3d binding energy spectrum, and (c) O 1s binding energy spectrum.

It is well-known that X-ray photoelectron spectroscopy (XPS) is a very useful method in determination of the chemical compositions and their chemical states of material surfaces. In our case, the XPS is applied to analysis the chemical composition of the hierarchical molybdenum oxide. The XPS survey spectrum for the obtained MoO_3 is shown in Figure Fig. **2** (a). The spectrum shows that the main constituent elements were

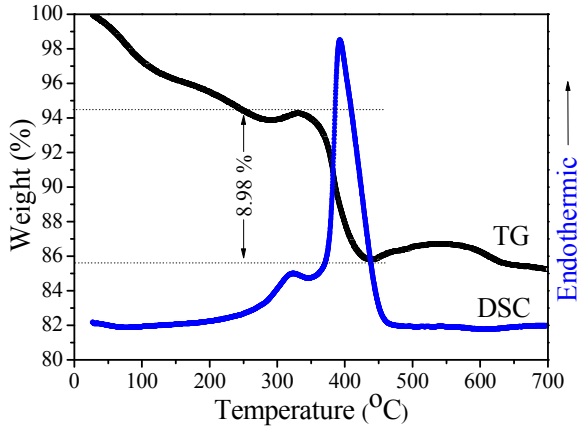

Fig. 3 TG-DSC curves of MoS_2 precursors.

molybdenum and oxygen atoms, except for additional peak resulting from carbon which is the charged correction calibration. High resolution spectra of Mo3d and O1s photoelectron lines for hierarchical MoO_3 surface were recorded show in Fig. 2(b) and (c).The Mo3d core level spectrum recorded on hierarchical MoO_3 samples show two groups of Mo3d doublets. The two components associated with $Mo3d_{5/2}$ and $Mo3d_{3/2}$ spin orbit doublet at 232.3 and 235.5 eV respectively, are in agreement with those found in the literature for Mo^{6+} in MoO_3 stoichiometric.[24,25] And, the peak at 530.6 eV corresponds to the binding energy of the O1s. To demonstrate the formation mechanism of MoO_3 samples, the conversion of MoS_2 precursors during annealing treatment was also investigated by Thermogravimetric (TG) and differential scanning calorimetric (DSC) at a program-controlled temperature elevation rate of 10 °C min^{-1} in air. In Figure 3, an obvious weight loss in the TG curve accompanied with an exothermic peak in the DSC curve from 300 to 400 °C can be observed. It can be attributed to the drastic conversion of MoS_2 precursors in this condition. The net weight loss is about 8.98 wt %, which is close to the theoretical value for the substitution of S by O atoms from MoS_2 to MoO_3, further supporting the oxidizing process of MoS_2 precursors.

The microstructure and morphology of the as-prepared MoS_2 precursors and hierarchical MoO_3 nanostructures were further characterized by FESEM and TEM. The surface morphology of the MoS_2 precursors could be clearly observed from typical FESEM images at different magnifications. As shown in Fig. 4(a) and (b), every MoS_2 nanostructures with an average diameter of 500 to 700 nm. Furthermore, the 3D nanostructures were consisted of many 2D nanosheets, which were tightly aggregated. MoO_3 samples can be obtained by annealing the MoS_2 precursors at 400 ºC. Clearly, the MoO_3 products inherit the morphology of their precursor, as shown in Fig. 4(c) and (d). The intriguing structure is also elucidated under TEM to provide further insight about the morphology and microstructure of the as-synthesized hierarchical MoO_3 nanostructures. In good agreement with the FESEM image, a low-magnification TEM image (Fig. 5(a)) of a single MoO_3 nanostructures. It can be seen that the MoO_3 nanostructures with the diameter of about 500 nm, which is constructed by relatively densely

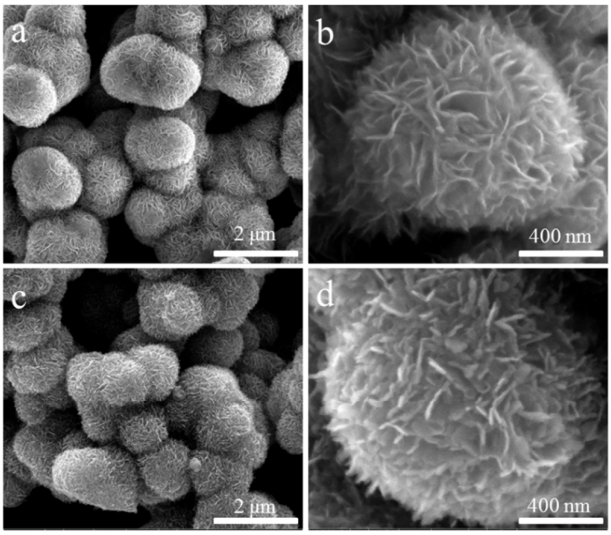

Fig. 4 (a and b) Typical FESEM image of MoS2 precursors and (c and d) hierarchical MoO3 nanostructures.

packed nanosheets. With a closer observation, the nanosheets are around 5-10 nm in thickness (Fig. 5(b)). The high-resolution TEM image (Fig. 5(c)) clearly displayed the lattice fringes with a constant spacing of 0.38 nm ascribed to the (110) plane of MoO_3. Moreover, the corresponding SAED pattern (Fig. 5(d)) confirms the polycrystallinity structure of hierarchical MoO_3 nanostructures and presents well-defined rings that can be well indexed to the XRD patterns.

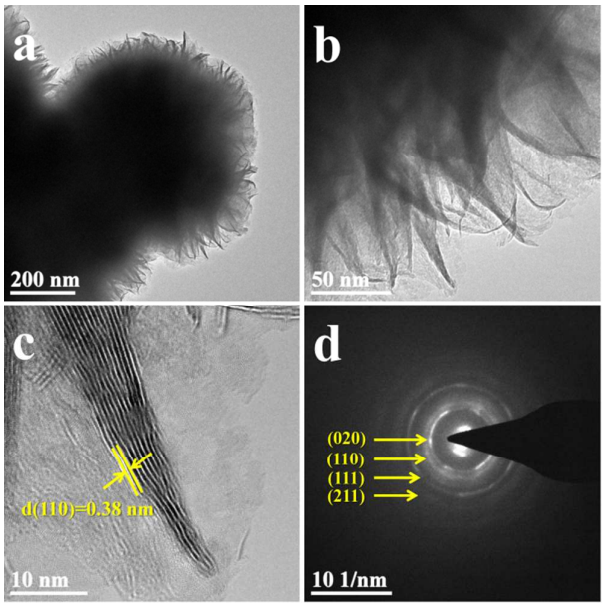

Fig. 5 (a) Low and (b) high magnification TEM image of hierarchical MoO_3 nanostructures; (c) the corresponding HRTEM image with labeled lattice spacing and (d) corresponding SAED pattern.

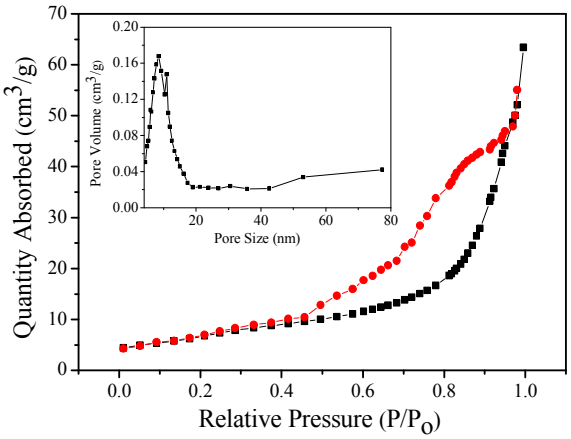

Fig. 6 Nitrogen adsorption-desorption isotherms of hierarchical MoO_3 nanostructures. The insets are pore size distributions.

In addition to the microstructure, the porosity and surface area of materials are important for their gas sensing properties. In order to investigate the porosity and surface area, BET nitrogen adsorption-desorption measurements were carried out on the hierarchical MoO_3 nanostructures. As shown in Fig. 6, the nitrogen adsorption-desorption isotherms are ascribed to type H4 with a distinct hysteresis loop, suggesting the mesoporous structure of the hierarchical MoO_3 nanostructures. From the pore size distribution curve (inset in Fig. 4), we can see that the pores with sizes of about 10 nm are dominant. The BET surface area of hierarchical MoO_3 nanostructures is 43.2 m^2/g. Since the as-prepared MoO_3 products possess large surface area and mesoporous structure, which are greatly advantageous for gas adsorption–desorption, gas molecular diffusion, and providing more surface sites for oxygen, it is believed that they can be potentially applied in gas sensors with enhanced gas-sensing performance.

Based on the above experimental results, we proposed a possible formation mechanism for hierarchical MoO_3 nanostructures, as

Fig. 7 Formation mechanism of hierarchical MoO_3 nanostructures.

shown in Fig. 7. In the formation process, sodium molybdate was chosen as the precursor for molybdenum and thioacetamide was used as the sulfur source. During the subsequent hydrothermal treatment, MoO_4^{2-} anions were reduced under high temperature condition, forming MoS_2 nanoparticles.[26,27] Subsequently, the nanoparticles started to assemble together and spontaneously aggregate into MoS_2 nanosheet structures in order to reduce the high surface energy through the process known as oriented aggregation. Then, well-defined MoS_2 nanoflowers are formed from many MoS_2 nanosheets through a self-assembly process.[28,29] Finally, the hierarchical MoO_3 nanostructures were transformed by hierarchical MoS_2 nanostructures at 400 °C under oxidizing atmosphere with the following reactions:

$$2MoS_2 + 7O_2 \rightarrow 2MoO_3 + 4SO_2 \quad (2)$$

Gas-sensing properties

Because the as-prepared hierarchical MoO_3 nanostructures assembled from nanosheets, a high fraction of the atoms should present at the surface. It is expected that hierarchical MoO_3 nanostructures would exhibit a superior gas sensing performance. Thus, we investigated their gas-sensing properties, using ethanol as the main target gas. It is well known that the operating temperature is an important parameter for the semiconductor oxide sensors.[30-32] Therefore, to find the optimum detection temperature, the responses of hierarchical MoO_3 nanostructures to 200 ppm ethanol were tested as a function of operating temperature. As shown in Fig. 8, the response of the sensor based on hierarchical MoO_3 nanostructures varied with operating temperature. And the sensor has an optimum operating temperature of 260 °C, at which the sensor exhibited the highest response of 80 to ethanol gas.

Fig. 9(a) shows the typical response of gas sensors based on hierarchical MoO_3 nanostructures to 50-1000 ppm ethanol at260 °C. It can be clearly seen that the response of the sensor increases with increasing concentration of ethanol. The response of semiconductor oxide of gas sensor can be empirically represented as $S = a[C]^b + 1$, where a and b are the constants and S is the gas response, C is the concentration of the test gas. Generally, the exponent b has an ideal value of 0.5 to 1, which is derived from the surface interaction between chemisorbed oxygen and reducing gas to n-type semiconductor.[33,34] Fig. **9**(b) shows a chart of logarithm of the response of the sensor (S-1) versus the logarithm of ethanol concentration (C). The linear fitting was quite good, and the value of b towards ethanol was about 0.7631, determined by the fit shown as the solid line in Fig. 5(b), which was in good agreement with the theory of power laws for semiconductor sensors.[35, 36]

Response and recovery times are also important parameters for gas sensors. Fig. 10 shows the dynamic response of the sensor based on hierarchical MoO_3 nanostructures to 200 ppm ethanol at 260 °C. It is evident that the response curves of the sensor increases sharply with increasing concentration of ethanol and then returns to the baseline quickly with the ethanol exhausted out in the closed testing chamber, indicating their quick and reversible response and recovery time. For 200 ppm ethanol gas, 16 s and 10 s are the response and recovery time for hierarchical MoO_3 nanostructures, respectively. For the gas sensing mechanism of as-prepared hierarchical MoO_3 nanostructures, it should belong to the

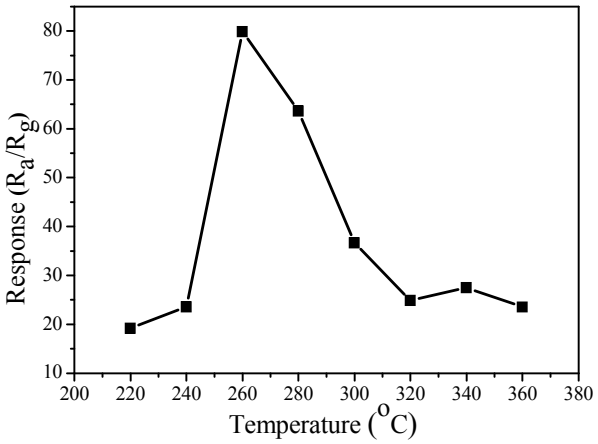

Fig. 8 Response of hierarchical MoO_3 nanostructures to 200 ppm ethanol as a function of operating temperature.

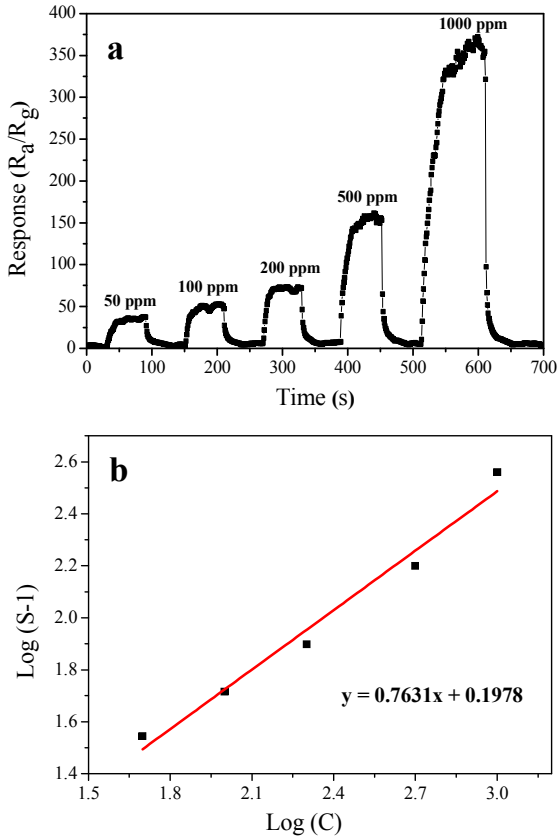

Fig. 9 (a) Typical response curves and variation of the response of hierarchical MoO_3 nanostructures exposed to different concentration of ethanol ranging from 50 to 1000 ppm and measured at 260 °C; (b) the corresponding log (S-1) *vs*. log (C).

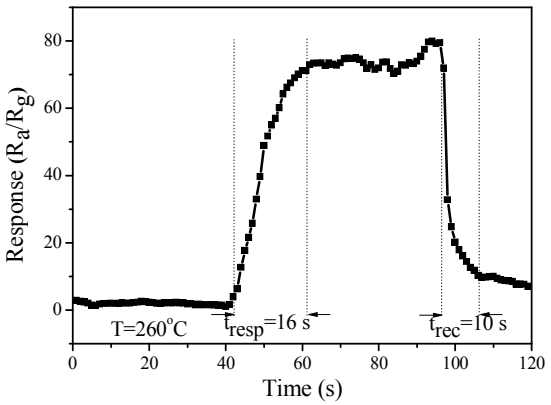

Fig. 10 Response and recovery time of the sensor based on hierarchical MoO_3 nanostructures to 200 ppm ethanol at 260 °C.

surface-controlled type, which may be explained by the change in resistance of the sensor upon exposure to different gas atmospheres. When the sensors were exposed to air, O_2 adsorb on the surface and create chemisorbed oxygen species (such as O_2^-, O^- and O^{2-}) by capturing electrons from the conductance band. When the sensors exposed to ethanol vapor at higher temperature, ethanol reacts with the adsorbed oxygen ions reducing their concentration and thereby increasing the semiconductor conductivity. The possible reactions took place on the surface of indium oxide as follows:[37,38]

$$CH_3CH_2OH + 3O^{2-}_{ads} \rightarrow 2CO_2 + 3H_2O + 6e^- \quad (3)$$

When exposed to air again, the sensor based on hierarchical MoO_3 nanostructures recovered to the initial electronic structure.

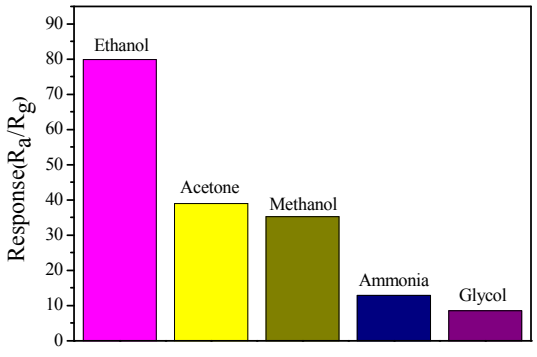

Fig. 11 Responses of hierarchical MoO_3 nanostructures five kinds of target gases (200 ppm) at a working temperature of 260 °C.

Gas sensing selectivity is one of the most important properties for the gas sensors. Fig. 11 shows the gas sensing response of hierarchical MoO_3 nanostructures five kinds of target gases (200 ppm) at a working temperature of 260 °C. Clearly, the sensor response to ethanol is much higher than that of acetone, methanol, ammonia, and glycol. Consequently, it is concluded that the sensor based on the as-prepared hierarchical MoO_3 nanostructures shows good selectivity toward ethanol and it maybe have potential applications in the detection of ethanol vapors.

The hierarchical MoO_3 nanostructures based sensor exhibits excellent reproducibility. Fig. 12(a) shows that the sensor is maintained at its initial response amplitude without obvious fluctuations upon three successive sensing tests for 100 ppm ethanol at 260 °C. Furthermore, the stability of the sensor was also determined at 260 °C for 3 days, as shown in Fig. 12(b). The senor has nearly constant response to 100 ppm ethanol, which confirmed the high stability of the sensor based on hierarchical MoO_3 nanostructures. In addition, a comparison between the sensing

Table 1 Gas-sensing property of various MoO_3 nanostructures to ethanol in the literatures and present study.

Sensing MoO_3 nanostructures	Operating temperature (°C)	Ethanol concentration (ppm)	Sensor response	Ref
Hierarchical MoO_3 nanostructures	260	200	80	This work
MoO_3 nanobelts	300	200	~12	4
MoO_3 nanorods	280	1000	40	39
MoO_3 hollow microspheres	270	200	~18	40
MoO_3 hollow microtubules	240	200	36	41
Net-like MoO_3 porous architectures	350	200	~17	42
MoO_3 submicron belts	370	200	~15	43
MoO_3 nanoplates	300	200	~40	44

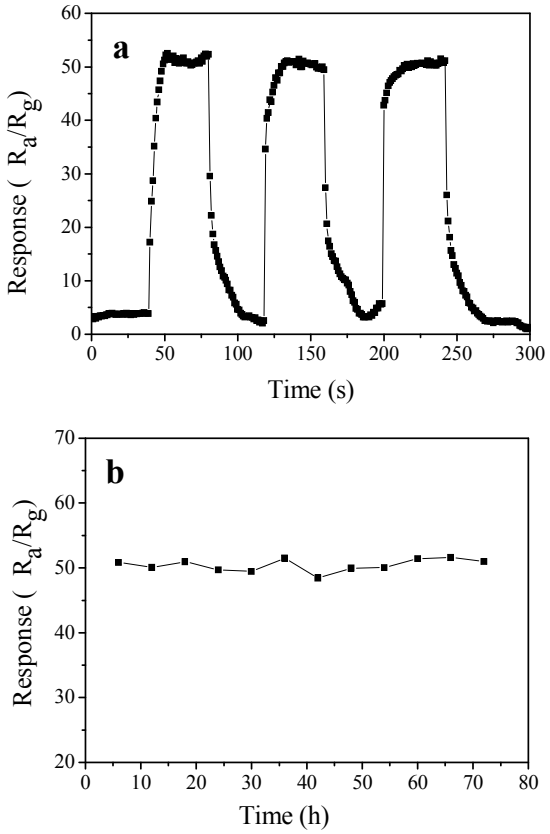

Fig. 12 Reproducibility of the sensor based on hierarchical MoO_3 nanostructures.

performances of the sensor and literature reports is summarized in Table 1. It is noteworthy that the sensor in our work exhibits higher response compared with other nanostructured MoO_3 sensors reported in previous works.[5, 37-42] The enhancement in gas-sensing properties on hierarchical MoO_3 nanostructures were attributed to the high surface area and 3D hierarchical architecture with well-aligned structures with a less agglomerated configurations, which could significantly facilitate gas diffusion and mass transportation in sensing materials. These results strongly proved that the prepared 3D hierarchical MoO_3 nanostructures are promising candidates for gas sensing applications.

Conclusions

In a summary, a facile and controllable hydrothermal approach combined with a subsequent annealing process was developed for the synthesis of hierarchical MoO_3 nanostructures, which were constructed by plenty of nanosheets with the thickness about 5-10 nm. Compared with other MoO_3 nanostructures, the sensing performance of the sensor based on hierarchical MoO_3 nanostructures exhibited enhanced response to ethanol. The improvement of sensing properties was attributed to the high surface area and 3D hierarchical structure. And the results suggest that the as-prepared hierarchical MoO_3 nanostructures are promising candidates for good performance ethanol sensor.

Acknowledgements

This work was financially supported by National Natural Science Foundation of China (No. 61102006 and 51172095), Natural Science Foundation of Shandong Province, China (No. ZR2015EM019 and ZR2014EL006), and Shandong Province Higher Educational Science and Technology Program (No. J15LA56).

Notes and references

1 A. Tricoli, M. Righettoni, A. Teleki, *Angew. Chem. -Int Edit*, 2010, **49**, 7632-7659.
2 J.Q. Xu, D. Wang, L.P. Qin, W.J. Yu, Q.Y. Pan, *Sensor. Actuat. B*, 2009, **137**, 490-495.
3 M. Tiemann, *Chem. Eur. J.*, 2007, **13**, 8376-8388.
4 G.E. Buono-Core, A.H. Klahn, C. Castillo, et al. *J. Non-Cryst. Solids*, 2014, **387**, 21-27.
5 Y. Ma, X. Zhang, M. Yang, Y. Qi. *Mate. Lett*., 2014, **136**, 146-149.
6 S.M. Wang, B.X. Xiao, T.Y. Yang, et al. *J. Mate. Chem. A*, 2014, **2**, 6598-6604.
7 M.B. Rahmani, S.H. Keshmiri, J. Yu, et al. *Sens. Actuators, B*, 2010, **145**, 131-9.
8 H.M. Martínez, J. Torres, M.E. Rodríguez-García, et al. *Physica B*, 2012, **407**, 3199-3202.
9 K. Khojier, H. Savaloni, S. Zolghadr. *Appl. Surf. Sci*., 2014, **320**, 315-321.
10 E. Comini, L. Yubao, Y. Brando, G. Sberveglieri, *Chem. Phys. Lett*., 2005, **407**, 368-371.
11 J. Gong, W. Zeng, H. Zhang. *Mate. Lett*., 2015, **154**, 170-172.
12 W.S. Kim, H.C. Kim, S.H. Hong. *J. Nanopart. Res*., 2009, **12**, 1889-1896.
13 S.L. Bai, C. Chen, Y. Tian, S. Chen, R.X. Luo, D.Q. Li, A.F. Chen, C.C. Liu, *Mater. Res. Bull.*, 2015, **64**, 252-256.
14 W.S. Kim, H.C. Kim, S.H Hong, *J Nanopart Res*, 2010, **12**, 1889-1896.
15 H.K. Wang, A.L. Rogach, *Chem. Mater.*, 2014, **26**, 123-33.
16 D. Han, P. Song, H.H. Zhang, et al. *RSC Adv*., 2014, **4**, 50241-50248.
17 X.X Wang, K. Tian, H.Y. Li, et al. *RSC Adv*., 2015, **5**, 29428-29432.
18 X.W. Li, C. Wang, X. Zhou, et al. *RSC Adv*., 2014, **4**, 47319-47324.
19 J.H. Lee. *Sens. Actuators, B*, 2009, **140**, 319-336.
20 L.L. Wang, T. Fei, Z. Lou, T. Zhang, *ACS Appl. Mater. Interfaces*, 2011, **3**, 4689-4694.
21 Z.D. Lin, F. Guo, C. Wang, X.H. Wang, K. Wang, Y. Qu, *RSC Adv*, 2014, **4**, 5122-5129.
22 S. Agarwala, Z.H. Lim, E. Nicholson, G.W. Ho, *Nanoscale*, 2012, **4**, 194-205.
23 S. Agarwala, W.L. Ong, G.W. Ho, *Sci. Adv. Mater.*, 2013, **5**, 1418-1426.
24 S.S. Sunu, E. Prabhu, V. Jayaraman, et al. *Sensor. Actuat. B,* 2004, **101**, 161-174
25 J.C. Dupin, D. Gonbeau, P. Vinatier, A. Levasseur, *Phys. Chem. Chem. Phys.,* 2002, **2**, 1319-1332
26 Y.D. Li, X.L. Li, R.R. He, J. Zhu, Z.X. Deng, *J. Am. Chem. Soc.*, 2002, **124**, 1411-1416.
27 C. Pacholski, A. Kornowski, H. Weller, *Angew. Chen. –Int Edit*, 2002, **41**, 1188-1191.

28 G.G. Tang, J.R. Sun, C. Wei, et al. *Mater. Lett*., 2012, **86**, 9-12.
29 Y. Cheng, Y.S. Wang, Y.H. Zheng, Y. Qin, J. *Phys. Chem. B*, 2005, **109**, 11548-11551.
30 Z. Lou, L.L. Wang, T. Fei, T. Zhang, *New J. Chem*., 2012, **36**, 1003-1007.
31 L.J. Bie, X.N. Yan, J. Yin, Y.Q. Duan, Z.H. Yuan, *Sens. Actuators B*, 2007, **126**, 604-608.
32 P. Sun, X. Zhou, C. Wang, K. Shimanoe, G. Lu, N Yamazoe, *J. Mater. Chem. A*, 2014, **2**, 1302-1308.
33 M. Arienzo, L. Armelao, C.M. Mari, S. Polizzi, R. Ruffo, R. Scotti, F. Morazzoni, *J. Am. Chem. Soc.*, 2011, **133**, 5296–5304.
34 L.X. Zhang, J.H. Zhao, H.Q. Lu, L. Li, J.F. Zheng, H. Li, Z.P. Zhu, *Sensor. Actuat. B*, 2012, **161**, 209-215.
35 N. Yamazoe, K. Shimanoe, *Sensor. Actuat. B*, 2008, **128**, 566-573.
36 X.J. Liu, Z. Chang, L. Luo, X.D. Lei, J.F. Liu, X.M. Sun, J. Mater. Chem., 2012, **22**, 7232-7238.
37 J.Q. Xu, J.J. Han, Y. Zhang, Y.A. Sun, B. Xie, *Sensor. Actuat. B*, 2008, **132**, 334-339.
38 H. Men, P. Gao, B.B. Zhou, Y.J. Chen, C.L. Zhu, G. Xiao, L.Q. Wang, M.L. Zhang, *Chem. Commun*., 2010, **46**, 7581-7583.
39 X.F Chu, S. Liang, W. Sun, et al. *Sensor. Actuat. B*, 2010, **148**, 399-403.
40 X. Zhao, M. Cao, C. Hu. *Mater. Res. Bull.*, 2013, **48**, 2289-2295.
41 P. Song, Q. Wang, J. Li, et al. *Sensor. Actuat. B*, 2013, **181**, 620-628.
42 W. Zeng, H. Zhang, Y.Q. Li, et al. *J. Mater. Sci*., 2014, **25**, 338-342.
43 T. Yunusi, C. Yang, W.L. Cai, et al. *Ceram. Int*., 2013, **39**, 3435-3439.
44 D.L. Chen, M.N. Liu, L. Yin, et al. *J. Mater. Chem*., 2011, **21**, 9332-9342.